Pergamon

Int. J. Multiphase Flow Vol. 24, No. 3, pp. 431–452, 1998

Printed in Great Britain

PII: S0301-9322(97)00067-0

0301-9322/98 $19.00 + 0.00

A STUDY OF THE BUBBLE-TO-SLUG TRANSITION IN VERTICAL GAS-LIQUID FLOW IN COLUMNS OF DIFFERENT DIAMETER

H. CHENG, J. H. HILLS and B. J. AZZORPARDI

Department of Chemical Engineering, University of Nottingham, Nottingham NG7 2RD, England

(Received 25 September 1996; in revised form 1 September 1997)

Abstract—The aim of this study is to investigate the structure of upwards air-water flow and its variation as the bubble-to-slug transition is approached, with a view to understanding the mechanism of the transition. The development of bubble size with column height is measured with a double needle resistivity probe, and of void fraction waves with an Impedance Void Fraction Meter (IVFM) with quadrant electrodes in a 150 mm diameter column. The results are compared with some experimental data gathered in a 28.9 mm column. Traditional slug flow does not exist in the 150 mm diameter column; instead there is a gradual transition to churn flow. Possible instabilities of void fraction waves are detected during the transition from bubble to churn at constant liquid rate, but not at constant gas rate. In the 28.9 mm column at constant liquid rate, an abrupt transition from bubble-to-slug flow occurs, with strong indications of associated void fraction wave instabilities. © 1998 Elsevier Science Ltd. All rights reserved

Key Words: bubble-to-slug transition, vertical gas-liquid airflow, column diameter

1. INTRODUCTION

Systems involving gas-liquid two-phase flows are found widely in the process, chemical, nuclear power, petroleum and related industries. In gas-liquid two-phase concurrent vertical flow, there are a number of different flow regimes, of which the most important are bubble, slug, churn and annular. These regimes are important in themselves (the slug and churn regimes have large pressure fluctuations which can damage equipment), and also because of their influence on heat and mass transfer phenomena; thus, the first stage in analysing a two-phase flow is usually to determine the prevailing flow regime. This requires an understanding of the factors influencing the transition between regimes, and as part of a larger project looking at all the transitions, this paper concentrates on the flow from bubble to slug.

Bubble flow is characterised by bubbles which are small compared to the tube diameter, dispersed more-or-less randomly in the liquid continuum within the tube, while slug flow is characterised by Taylor bubbles separated by slugs of continuous liquid.

A Taylor bubble is a constant pressure surface, whose shape is that of a cylinder bounded on top by a spherical cap or a bullet shaped nose, and at the bottom by a distorted flat tail. The mean diameter of the bubble cylinder is almost equal to the tube diameter, and the length is at least one tube diameter. Between the Taylor bubble and the pipe wall, liquid flows downward in the form of a thin falling film, and there are often small bubbles in the slug of liquid following the Taylor bubble.

In early 1960s, Radovcich and Moissis (1962) suggested that the bubble-to-slug transition is due to collisions between small bubbles, with a fraction of these collisions resulting in coalescence, ultimately leading to bubbles which are of similar diameter to the pipe and hence to slug flow. Bubble flow is thus only a transient flow regime, which, given a sufficiently long residence time in a pipe, will develop into slug flow. Because the rate of collision increases dramatically at void fractions of 0.25–0.3, they suggested a void fraction criterion for the transition. Taitel *et al.* (1980) also claimed that gradual bubble coalescence is responsible for the transition to slug flow, but suggested a dispersed bubble flow pattern can be maintained if an equilibrium between bubble coalescence and break-up due to liquid turbulence is reached.

However, Hewitt (1990) found that there was no effect of channel length on the transition condition and void fraction, implying that the transition from bubble to slug occurs simultaneously throughout the channel, and making it unlikely that break-up and coalescence of the bubbles is the mechanism responsible for the transition. Similarly, Kapteyn (1989) measured bubble size and number density in bubble flow, and observed no differences in these parameters between the top and the bottom of his flow channel, suggesting no gradual coalescence of the type envisaged by Radovcich and Moissis (1962).

Some recent work has developed the suggestion, first made by Wallis (1969), that the bubble-to-slug transition is associated with instabilities of void fraction waves. Such waves have been studied extensively by workers in Grenoble and subsequently in many other laboratories, mainly using a series of Impedance Void Fraction Meters (IVFM) along the length of the test section. However, only some of the more recent papers cover the transition from bubble-to-slug flow (Matuszkiewicz *et al.* 1987; Kytömaa 1987; Tournaire 1987; Bouré 1988; Saiz-Jabardo and Bouré 1989; Kytömaa and Brennen 1991; Park 1992; Monji 1993; Park *et al.* 1993 Song *et al.* 1995a; Song *et al.* 1995b).

There are two main approaches to the experimental study of void fraction waves: a few workers generated small amplitude waves of different known frequencies and studied their propagation up the column (Micaelli 1982; Tournaire 1987; Saiz-Jabardo and Bouré 1989), while the majority investigated the behaviour of naturally occurring waves. The principal results are discussed below.

1.1. *Forced waves*

- At low void fractions (0.2 or below), all waves are damped, the extent of damping increasing with frequency. Any wave of frequency above a few Hz is strongly damped in all conditions. The upper frequency is typically 3 or 4 Hz, although in the experiments of Micaelli (1982) at high liquid velocity ($\rangle$1 m/s) it was more like 10 Hz, suggesting that there is probably a critical wavelength rather than critical frequency.
- For lightly-damped waves, the coherence between signals at successive measuring stations remains close to 1.0, but as damping takes effect, coherence falls away rapidly.
- At low void fractions, the wave velocity is independent of frequency (non-dispersive waves), and decreases slightly with increasing void fraction. It lies between the mean fluid velocity ($j_G + j_L$) and the mean bubble velocity j_G/α.
- As the void fraction is increased, a faster mode of kinematic wave appears, whose speed increases with void fraction; these waves are damped at high frequencies, but amplified at low frequencies, and seem to be associated with a clustering of the bubbles prior to coalescence and slug formation. When such amplification occurs, the coherence between successive signals is relatively high. These faster waves have a velocity greater than the mean bubble velocity j_G/α; Saiz-Jabardo and Bouré (1989) suggest that the appearance of such waves could be a non-subjective indicator of the transition from bubble to slug.

1.2. *Natural waves*

- In bubbly flow there is a broad power spectral density with a peak around 3 Hz. As the void fraction increases, the spectral density becomes sharper and moves to somewhat lower frequencies until, when the transition to slug flow occurs, a second peak appears at around 1 Hz.
- At lower void fractions, the standard deviation of the signal increases along the test section, while the system gain factor remains below 1.0 (i.e. wave attenuation). Matuszkiewicz *et al.* (1987) explain this apparent contradiction by saying that fresh disturbances are being created along the section (increasing the standard deviation) but they are also rapidly damped out. As would be expected, the coherence function between successive measuring stations is low in this range.
- At low void fractions, the wave velocity (calculated from the system phase factor) is constant along the section and independent of frequency; as the transition to slug flow is approached, it tends to increase towards the end of the test section and when slug flow develops it exhibits

a marked minimum: at the same time the gain factor becomes ≥ 1. The coherence function between successive observations also increases markedly as slug flow is approached.

- Park *et al.* (1993), working with a more viscous air/oil system, found the two modes of kinematic wave already noted in the forced wave study. Their velocities could only be obtained by cross-correlation: the system phase factor cannot yield information on two simultaneous waves, as was shown theoretically by Bouré (1988). The velocity of the faster wave was equal to the measured velocity of bubble clusters which were seen to form at quite low void fractions; this velocity rose with void fraction up to the transition to slug flow, after which it remained constant. These signals were lightly damped at low void fractions, but strongly amplified as the transition was approached.
- Working with air and water in a larger column (102 mm), Kytömaa and Brennen (1991) found a transition to churn-turbulent rather than to slug. Kinematic waves were always damped, but as the transition was approached, the minimum damping decreased dramatically, and the frequency at which it occurred also decreased suddenly. The wave velocity relative to the zero flux plane decreased with void fraction.
- Song *et al.* (1995a) investigated the effect of variable, controlled bubble size, using a bubble generator of the type developed by Serizawa *et al.* (1988) and Serizawa *et al.* (1991). Bubble size is known to affect the radial distribution of void fraction (Serizawa and Kataoka 1987) and also the void fraction at transition to slug flow (Liu 1993). In a 25 mm channel, they found that large bubbles ($\rangle$4 mm), which congregate in the centre of the channel, form clusters even at quite low void fractions, and as the void fraction increases, these clusters gradually coalesce along the channel into cap bubbles and finally slugs. The wave velocity increases regularly, and the gain factor of the dominant (least attenuated) frequency gradually increases, reaching 1 at about the transition. This behaviour is very similar to that of the faster wave of Park *et al.* (1993) and of Bouré (1988), both of whom associated it with "clusters" or "swarms" of bubbles.

Small bubbles ($\langle$4 mm), on the other hand, congregate near the tube walls, and show no tendency to form clusters, but simply become closer packed as the void fraction increases up to void fractions as high as 35%. At a certain void fraction, there is an abrupt coalescence throughout the channel to a churn-like structure, which with a further small increase in gas rate, leads to slug flow. Wave velocity decreases slightly with void fraction at low liquid rates (0.2 m/s) and increases slowly at higher rates, but there is always a sudden increase as the transition is reached. The gain factor of the dominant frequency remains low, and may even decrease as void fraction increases, but then jumps dramatically to a value of 1.0 at the transition. This behaviour shows similarities to that of the slower wave of Park *et al.* (1993) and of Bouré (1988), although these workers could not maintain the slow wave up to the transition.

Very similar behaviour was found in an 80 mm column (Song *et al.* 1995b), except that the small bubble transitions occurred at somewhat lower void fractions.

The purpose of this research is to make further investigations of the transition from bubbly flow, in an attempt to decide whether the instability of void fraction waves or a gradual coalescence process is the cause of the bubble-to-slug transition. This is achieved by measuring the variation of bubble properties (size, velocity and density distribution) with column height and also the propagation of void fraction waves along the column as the transition is approached. Bubble properties are determined using a double resistivity needle probe, and the void fraction waves are measured with an impedance void fraction meter.

In this paper, we present some experimental measurements of bubble property distributions at two different heights in a 150 mm diameter column, and of the propagation of void fraction waves both in the 150 mm column, and a smaller 28.9 mm diameter column.

2. EXPERIMENTAL SET-UP AND INSTRUMENTATION

2.1. *150 mm column*

The 150 mm diameter column is shown schematically in figure 1. It is essentially the equipment used by Hills (1976) with the addition of a liquid circulating pump. The riser and downco-

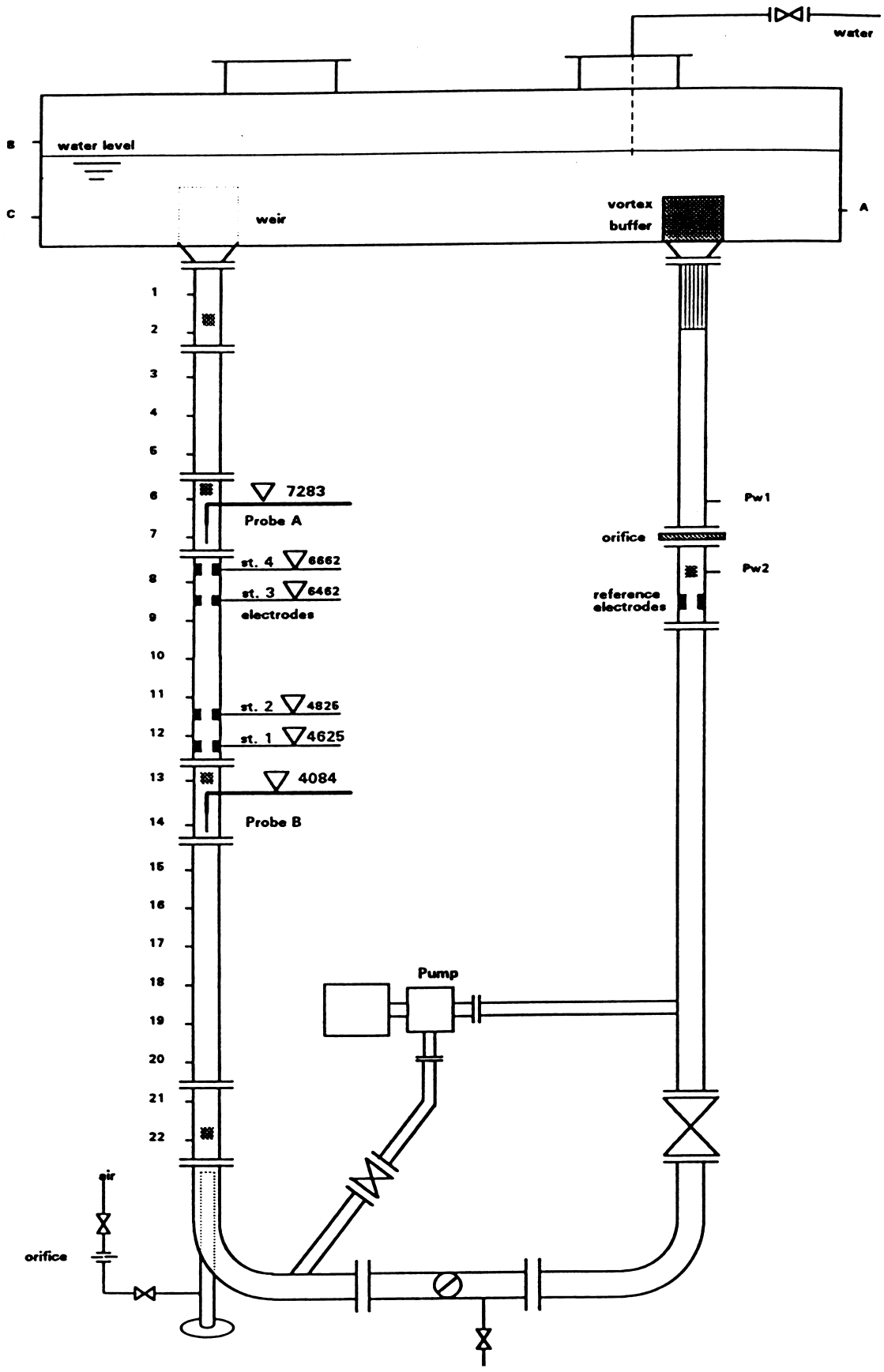

Figure 1. Experiment Rig (ID = 150 mm).

mer are constructed in u-PVC pipe of 150 mm internal diameter, and have a vertical straight section 10.5 m high. Five transparent sections are installed to observe the flow pattern in the riser and to check for air entrainment in the downcomer. A centrifugal pump is installed in the cross pipe between the riser and downcomer, so that the water flow rate can be varied independently, although in most of the experiments described here, the liquid was circulated by the gas-lift effect. Twenty-two pressure tappings are provided along the riser at 457 mm intervals, and are connected to manometers to estimate mean void fraction.

Compressed air from the laboratory air main enters the column through a 51 mm sparge cap at the foot of the riser. This sparge cap has 60×3.1 mm holes in the vertical cylindrical wall arranged in five banks of 12. Gas velocity is measured by an orifice plate in the feed line, and water velocity by an orifice plate in the downcomer.

Two different instruments are used in this column: a needle resistivity probe, and an impedance void fraction meter (IVFM). The double needle resistivity probe consists of two platinum wires of 0.1 mm diameter, insulated apart from their tips and fastened vertically alongside each other, with the tips about 5 mm apart in a vertical direction. The needle probe may be inserted at either of the two measuring stations (A and B) shown in figure 1.

The IVFM is similar to that used by Matuszkiewicz *et al.* (1987) and other workers. It consists of a pair of quadrant electrodes 20 mm high with 10 mm high guard electrodes on either side. The electrodes are made of 0.076 mm stainless steel sheet bent to the curvature of the column and glued to the inner wall. A reference electrode, of identical construction and situated in the downcomer serves to eliminate the effects of temperature variation on the conductivity of the water. The two electrodes are inserted into a Wheatstone's bridge operated at 5 kHz, and the out-of-balance voltage gives a measure of the voidage.

As shown in figure 1, four measuring electrodes are installed in the riser in two pairs; the two members of a pair (stations 1 and 2, and 3 and 4) are 20 cm apart, and the distance between 2 and 3 is 1.637 m. It was found experimentally that stations 20 cm apart are too close to allow meaningful measurements, so only the measurements at stations 2 and 3 will be presented in this paper.

The IVFM is calibrated *in situ* by averaging the signal electronically and comparing the value with the mean void fraction calculated from pressure measurements by ignoring frictional effects. Neglect of friction was justified by the observation that water velocity in the range 0–2 m/s had no noticeable effect on the calibration. Figure 2 gives the calibration curve, empirically fitted by:

$$V_\varepsilon - V_0 = 0.1798\varepsilon^2 + 0.3065\varepsilon$$

where V_ε and V_0 are the output voltages at void fractions of ε and zero, respectively.

2.2. *28.9 mm column*

The small diameter column has a clear acrylic riser 4.1 m high, with the main water flow circulated by a pump. A bubble generator similar in design to that of Serizawa *et al.* (1991) is placed at the base of the riser, so that bubble size can be varied, and the auxiliary water supply for this comes from the mains through a filter. Both main and auxiliary water flows, and the air flow from the laboratory mains are measured by rotameter. There are 14 pressure tappings along the riser at 300 mm intervals, which are connected to a manometer board.

Six equal-spaced measuring stations are used, with the first station at 0.55 m above the bubble generator. The distance between two successive measuring stations is 0.6 m. Each station is fitted with quadrant electrodes similar to those in the large column, except that they are flush-mounted on the inner wall of the test section in the 28.9 mm diameter column. Calibration was done in a similar manner to that in the 150 mm column, and again a quadratic equation was fitted to the result.

The data acquisition system, used for both needle probe and IVFM, consists of a 12 bit A/D converter (Data Translation, DT-2821) operated by DATS_plus software loaded on a personal computer. The output signals from both the needle probe and IVFM are statistically analysed using the DATS_plus package. For the needle probe, the sampling frequency is 25 kHz for each sensor (50 kHz for a double needle probe), and the sampling duration is 40–100 sec, depending

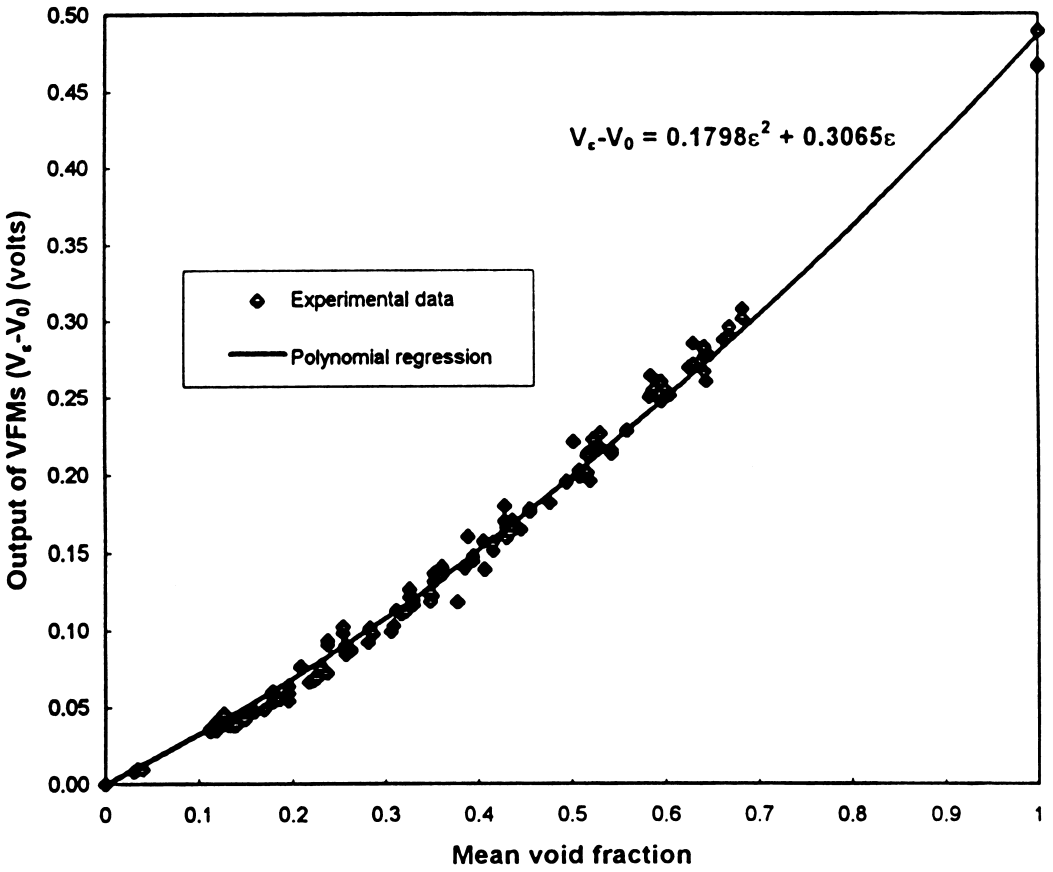

Figure 2. IVFM calibration in 150 mm column.

on flow conditions. For the IVFM measurements, the sampling frequency is 204.8 Hz and the sampling duration is 500 s.

3. EXPERIMENTAL CONDITIONS

Experimental measurements of both bubble size and void fraction wave have been completed in the 150 mm diameter column. A series of bubble size measurements have been carried out at stations A and B, 4 m and 7.2 m above the gas injector respectively, at constant water velocity of 0, 0.64 and 1.25 m/s; with mean void fractions measured by manometer in the range 0.06–0.41 at station A, and marginally higher at station B. The measurements of void fraction waves in the 150 mm diameter column are performed at three constant water velocities of 0, 0.32 and 0.65 m/s, with void fractions in the range 0.05–0.52, and at two constant gas velocities of 0.426 and 0.737 m/s, with mean void fractions covering a similar range.

In the 28.9 mm diameter column, void fraction wave measurements have been carried out at one constant water velocity of 0.65 m/s only, with the bubble generator run to produce a small bubble size (although the size has not yet been measured) and the mean void fraction varied from 0.073 to 0.3373 at the bottom and from 0.09995 to 0.4273 at the top.

In all cases, the void fraction range should cover the reported values for the bubble-to-slug transition.

4. DATA PROCESSING FOR BUBBLE SIZE MEASUREMENTS

The raw signals from the needle probe are not square-waves. They are processed by the method developed by Serizawa (1984), based on derivatives of the original signal truncated to eliminate spurious noise. We use the DATS_plus package to perform the differentiation and

truncation numerically. The four output files generated by the package contain the times of the rising signals and falling signals from the two needles. They are analysed by a series of discrimination programmes written in Quick BASIC.

First, the data from each needle is examined to check that "rise" and "fall" signals alternate, and to reject two successive "rise" or "fall" signals. At this stage, data from the upstream probe, felt to be more reliable, are analysed for bubble frequency and void fraction.

For a double needle probe with the two sensors separated by a known distance, bubble velocity can be determined from the time displacement of the interface. There are two methods used in the literature to determine the time lag of a travelling bubble. One is the cross-correlation technique, which gives the most probable time lag over the whole population sampled, and the other is the direct time delay measuring technique, which gives the spectrum of the time lags of individual bubbles. In our study, the latter method is adopted as it gives information on the bubble size and velocity spectra.

For the direct time delay measuring technique, the essential requirement is to identify the two corresponding signals for the same bubble, detected by both upstream and downstream sensor. Four criteria are set in a discrimination programme: if two signals from the double needle probe satisfy the four criteria simultaneously, they will be paired up.

1. The registered time at downstream needle should be later than the corresponding time at upstream needle for the same bubble.
2. Maximum and minimum time delays were selected to exclude the outlying points of the velocity distribution.
3. Bubble time chord lengths (the time duration when the bubble is in contact with the sensor) from upstream sensor and downstream sensor should agree within a reasonable range:

$$\frac{\Delta T_{\text{gas downstream}}}{a_2} > \Delta T_{\text{gas upstream}} > \Delta T_{\text{gas downstream}} \cdot a_2$$

4. Needle contacting time with water after a paired bubble (time duration between two successive bubbles) from upstream and downstream probes should agree within a reasonable range:

$$\frac{\Delta T_{\text{water downstream}}}{a_1} > \Delta T_{\text{water upstream}} > \Delta T_{\text{water downstream}} \cdot a_1$$

The choice of values of a_1 and a_2 is a compromise between high values, which risk accepting false pairs of signals, and low values, which, by rejecting a large number of true pairs may unduly bias the sample. After some experimentation, we chose $a_1 = 6$ and $a_2 = 8$. As a check, one set of experimental data have been re-processed with $a_1 = 2$ and $a_2 = 2$. Although the absolute values of bubble mean chord length at each radial position are larger than those found with $a_1 = 6$ and $a_2 = 8$, the trend of bubble chord length with column height remained the same.

Bubble frequency is measured by counting the number of bubbles at the upstream probe for a given time duration. The ratio of the time duration while the probe tip is in contact with gas phase to the total sampling time is taken as the local void fraction. Bubble velocity is decided from the averaged time displacement of liquid-gas interface and gas-liquid interface for a bubble passing through the double sensors. Bubble chord length is calculated from bubble velocity and bubble contacting time with the upstream probe for each individual bubble.

5. STATISTICAL DATA ANALYSIS FOR VOID FRACTION WAVES

The instantaneous signals from two successive measuring stations are simultaneously measured and then statistically processed, to determine the probability density function (PDF), the power spectral density function (PSD), cross-spectral density function (CSDF), coherence function, system gain factor, system phase factor, signal-to-noise ratio (SNR) and cross-correlation function. These quantities are used in the sense defined by Bendat and Pierson (1971).

All the analyses are performed by the DATS_plus package, by applying a Fast Fourier Transform (FFT) to the digitised fluctuating components. The PDF and the PSD give direct useful information on the flow structure, as does the SNR, defined as the standard deviation of the instantaneous void fraction signal normalised by its mean value. The magnitude and phase of the CSDF yield the coherence function, the system gain factor and system phase factor between signals. The wave propagation velocity can be found from the time lag, either determined from the system phase factor, or from the peak in the cross-correlation function. Because the void fraction waves are non-dispersive, the wave propagation velocities determined from cross-correlation and system phase factor in the 150 mm diameter column agree well. For the 150 mm column, only the data from the cross-correlation will be presented.

6. RESULTS AND DISCUSSION

6.1. *Measurements of bubble size and velocity in 150 mm diameter column*

Surprisingly, the effect of column height on the radial distribution of local bubble properties does not show any significant difference for different flow conditions, in spite of the variation of flow pattern. Therefore we only describe the observations at a water velocity of 0.64 m/s and present one set of typical results measured at a water velocity of 0.64 m/s and gas velocity of 0.552 m/s. The sampling time at this flow condition is 60 sec.

At constant water velocity of 0.64 m/s, with increasing gas velocity from 0.096 to 1.113 m/s, a number of flow configurations are observed by the naked eye. At a void fraction of 0.059, a uniform bubble flow was observed. Occasional cap bubbles appear at a void fraction of 0.131, and these increase in number as the void fraction increases to 0.171. At void fractions of $0.248 \sim 0.3939$, areas of high gas voidage separated by liquid slugs with low void fraction are observed. The liquid slugs with low void fraction are sometimes lifted by the fast moving big gas voidages and then re-bridge the column again. Near the wall, liquid containing small bubbles may move upwards, downwards and sometimes alternate its moving direction. Periodical pressure fluctuations generated by the alternate passage of liquid slugs and big gas voidages are observed in the manometers, which is a characteristic of traditional slug flow where Taylor bubbles appear. But these big gas voidages do not have a closed smooth surface like the traditional slug flow in small pipes, and they expand with increasing column height. The length of these voidages increases with increasing gas velocity at constant water velocity. The flow is chaotic, turbulent and fast. This is more like the churn flow of third kind defined by Hewitt and Jayanti (1993) rather than slug flow.

Typical bubble frequency distributions at two different heights are presented in figure 3(a). Surprisingly, local bubble frequency increases with height, which indicates that bubble break-up has happened in the interval from 4 m to 7.2 m above the gas inlet. Because of the coarse size of the holes in the gas distributor (3.1 mm) which was designed to simulate an industrial sparger, the initial bubble size is probably large, and it is not unlikely that bubble break-up could occur, but it is remarkable that it is occurring at a void fraction where coalescence might be expected.

Local void fraction distributions at the same flow condition at these two different heights are shown in figure 3(b). Local void fraction increases with increasing height, but this may be due to the fact that the absolute pressure decreases with column height, and hence superficial gas velocity increases.

The local mean bubble velocity is calculated from the velocity spectrum, and its distribution at these two different heights is displayed in figure 3(c). From this figure it is concluded that local mean bubble velocity increases with increasing height; this could again be due to the increased gas velocity due to expansion.

The local bubble chord length is calculated from bubble chord length spectrum. In order to allow for the effect of decreasing pressure with height, the distributions of bubble chord length at the two heights are corrected to 1 atm pressure by assuming that the air is ideal gas and the bubbles are spherical; the results are presented in figure 3(d). The distribution of median chord length is also shown in this figure; it could be more reliable as the mean is affected by the oc-

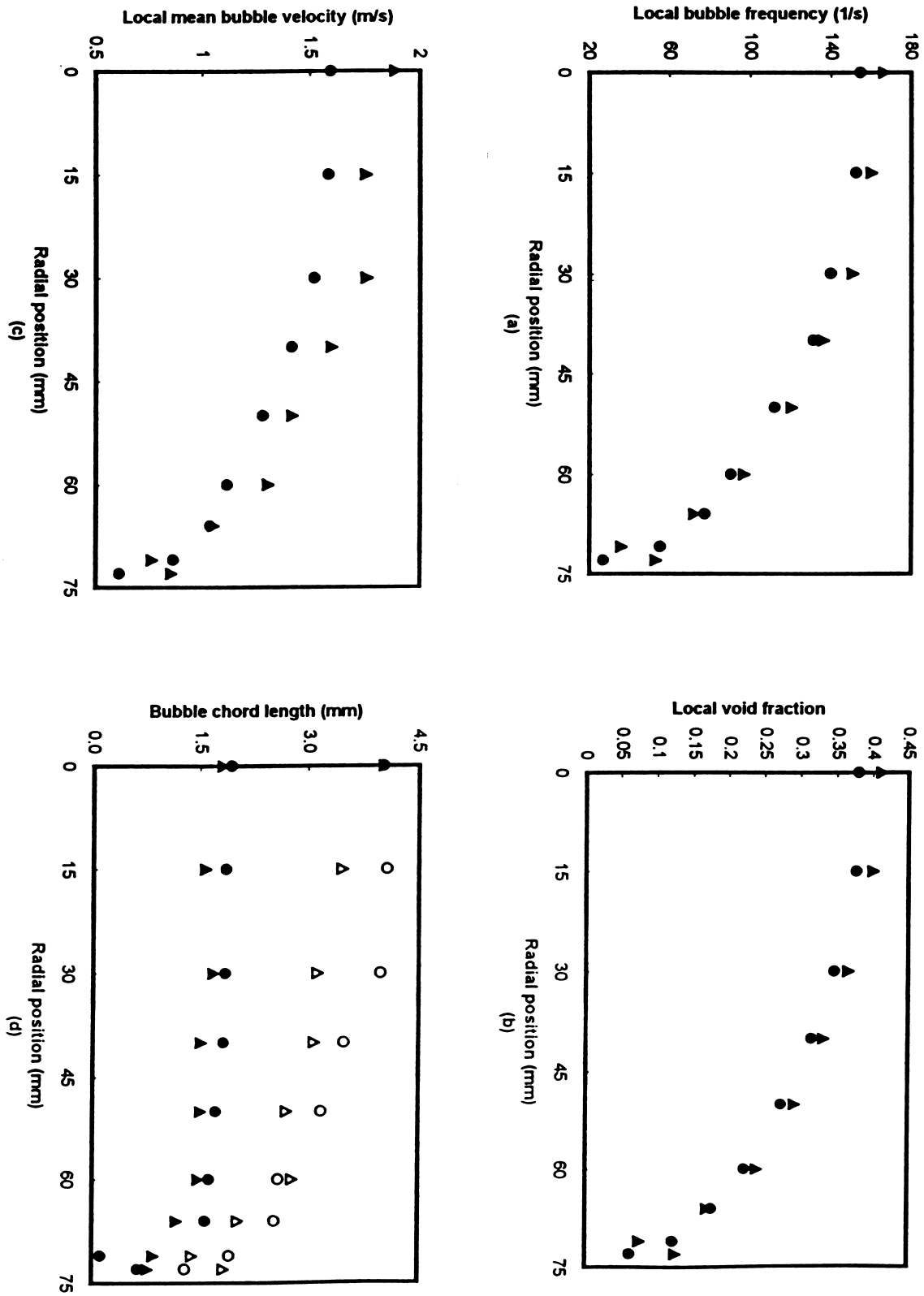

Figure 3. Variations of local properties with heights, (a) bubble frequency, (b) void fraction, (c) bubble velocity, (d) bubble chord length. Circles: 4 m above gas inlet; triangle: 7.2 m above gas inlet. In (d) solid symbols are for the median and open ones for the mean.

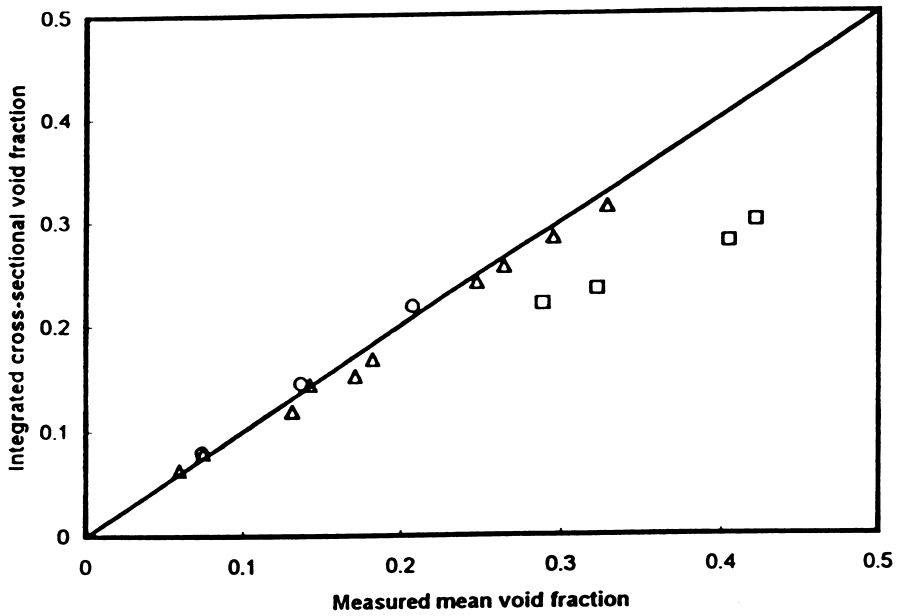

Figure 4. Comparison between measured and integrated void fraction. circle: at water velocity of 1.25 m/s, triangle: at water velocity of 0.64 m/s, square: at water velocity of 0.0 m/s.

casional large bubble. Both mean and median bubble chord length appear to decrease with increasing column height, confirming the conclusion that bubble break-up is occurring.

However, if the maximum bubble chord length is considered (corresponding to observed cap bubbles), it seems to increase somewhat with height, suggesting the possibility of growth of these large bubbles by coalescence, although the evidence is by no means conclusive.

For all the experimental conditions investigated, the comparison between measured void fraction by manometer and the integrated cross-sectional averaged void fraction at the two heights is shown in figure 4, and the comparison between the superficial gas velocity measured by orifice plate and the integrated cross-sectional averaged gas velocity at the two heights (corrected to

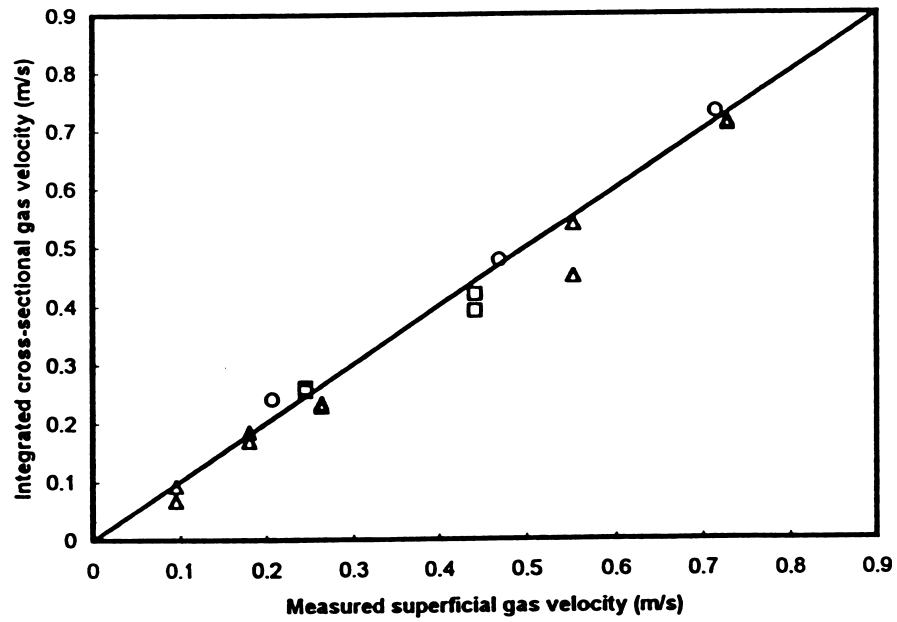

Figure 5. Comparison between measured and integrated gas velocity. For keys see figure 4.

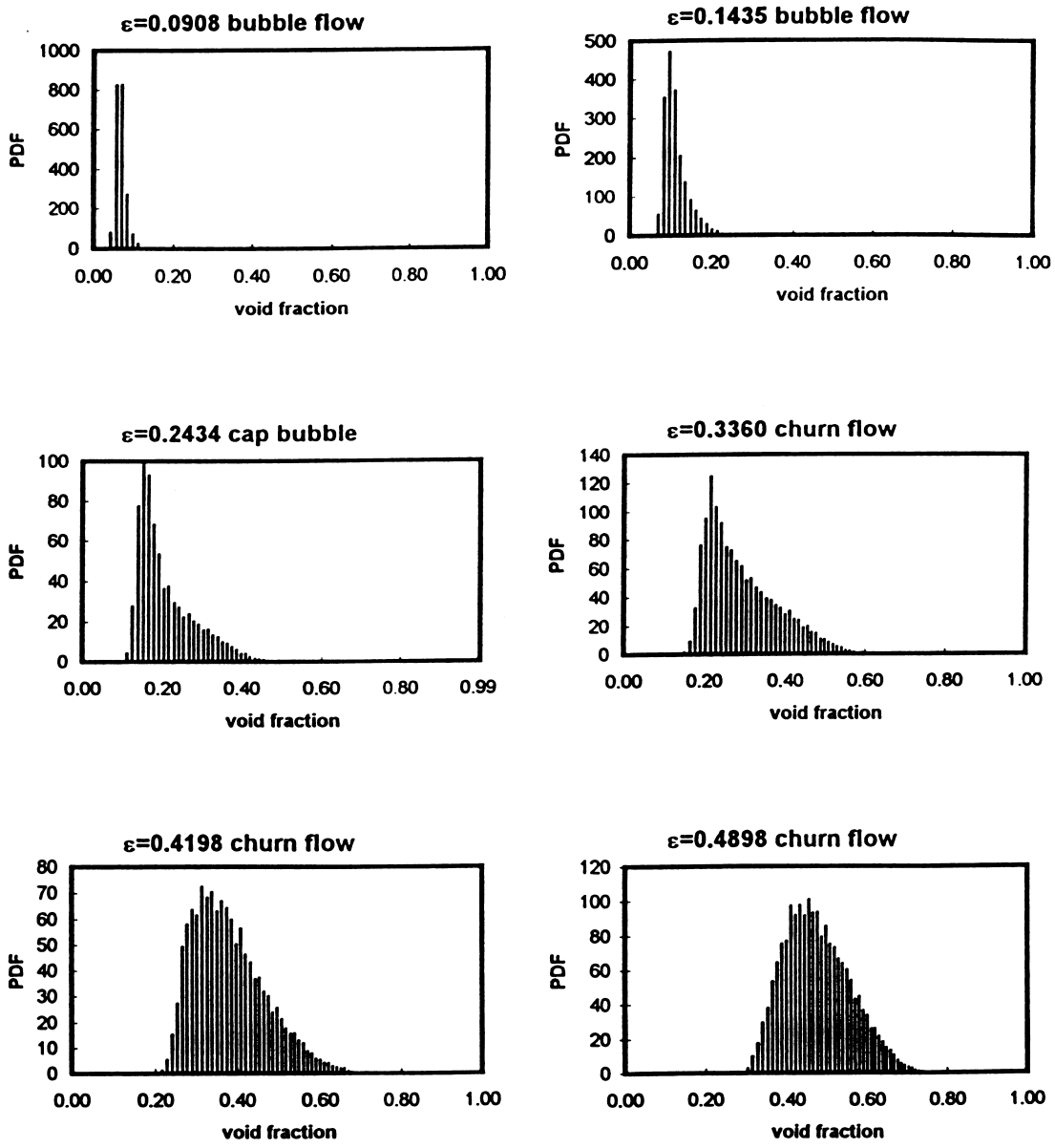

Figure 6. PDF plots at water velocity of 0.65 m/s.

standard conditions) is shown in figure 5. At zero liquid flow, where the bubbles and liquid may move down as well as up, the error in void fraction is significant, which indicates that the double needle probe is only suitable in situations where the bubbles move upwards. However, for the other flow conditions the error is very reasonable, which has substantiated the reliability of the double resistivity needle probe.

6.2. *Measurements of void fraction waves at constant water velocity in 150 mm column*

It is well-known that the PDF of void fraction shows two peaks for stable slug flow in a small pipe (Song *et al.* 1995a); one peak represents the void fraction in liquid slugs and another peak represents the void fraction in gas slugs. However, during the development of the flow pattern from bubble flow to slug-like or churn flow in the 150 mm diameter column, as shown in figure 6, the PDF of void fraction is single peaked for all flow conditions studied, moving to higher void fraction as the mean void fraction is increased. This confirms the earlier observation that there is no slug flow in this column, with the flow pattern in the column varying from dis-

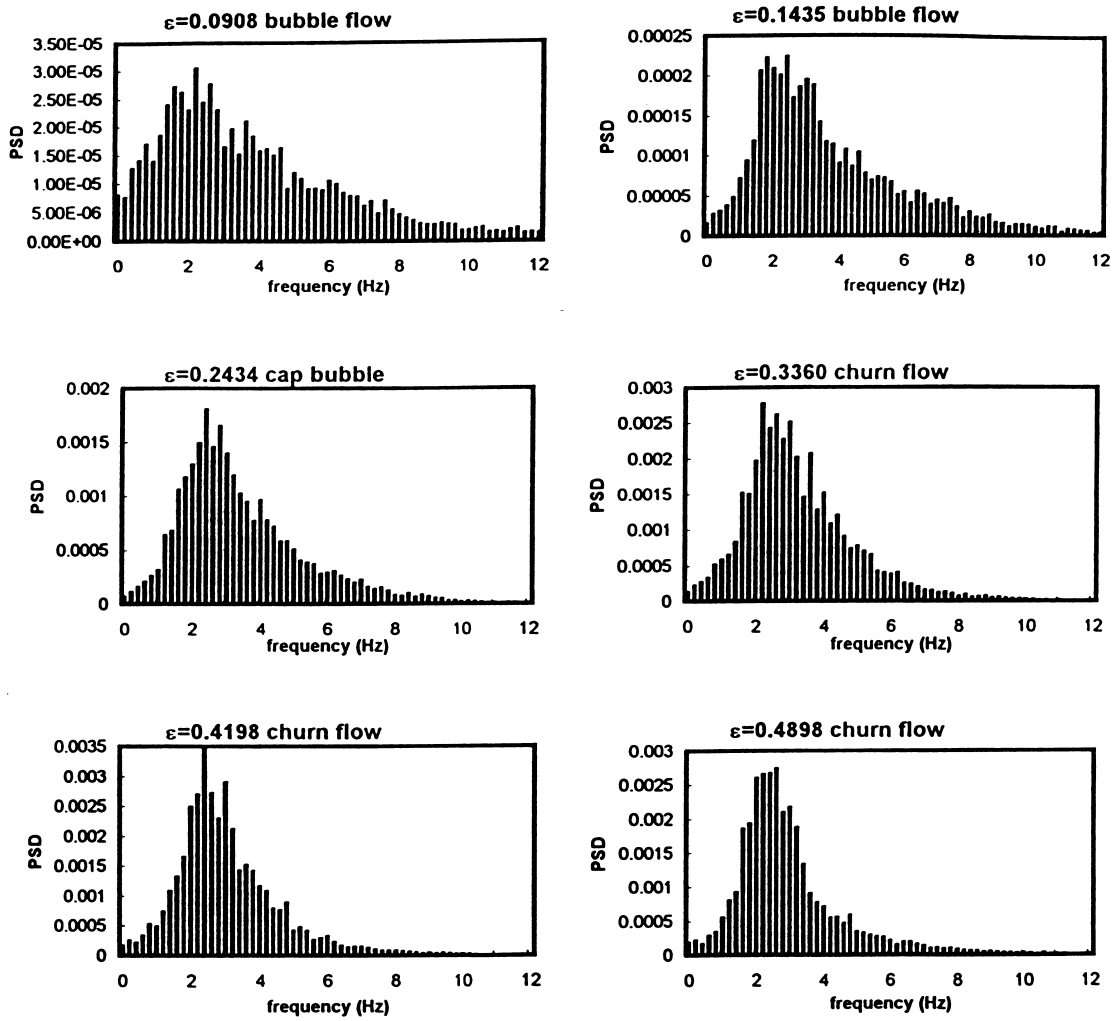

Figure 7. PSD plots at constant water velocity of 0.65 m/s. (Note the change in vertical scale).

crete bubble flow, through cluster bubble flow, cap bubble flow to churn flow as the gas rate is increased at constant liquid rate.

Bubble flow is observed for void fractions less than 0.2 in the 150 mm diameter column. For discrete bubble flow, the PSD of the void fraction signal does not show a peak, but from bubble cluster flow onwards, there is a distinctive peak in the PSD and the dominant frequency, which corresponds to the peak in the PSD, seems to remain unchanged as the void fraction is increased. The variation of PSD with mean void fraction at the three constant water velocities is similar; the results for UL = 0.65 m/s are illustrated in figure 7.

Wave velocity, determined from the peak time of the cross-correlation function, increases gradually with mean void fraction, as shown in figure 8. The graph also plots the dominant frequency (the peak frequency in the PSD curves of figure 7) and demonstrates that it is essentially constant. Thus the regions of high void fraction, which would become slugs in a narrower column, remain constant in number, but increase in velocity and hence wave length, as void fraction increases.

The development of SNR with mean void fraction at three constant water velocities is shown in figure 9. At each water velocity the SNR goes through a maximum as the flow pattern changes from bubble-to-churn flow; at the left-hand side of the maximum, it is a bubble flow, at the right-hand side it is a churn flow, and the maxima are consistent with the visual observation of cap bubble flow for each condition.

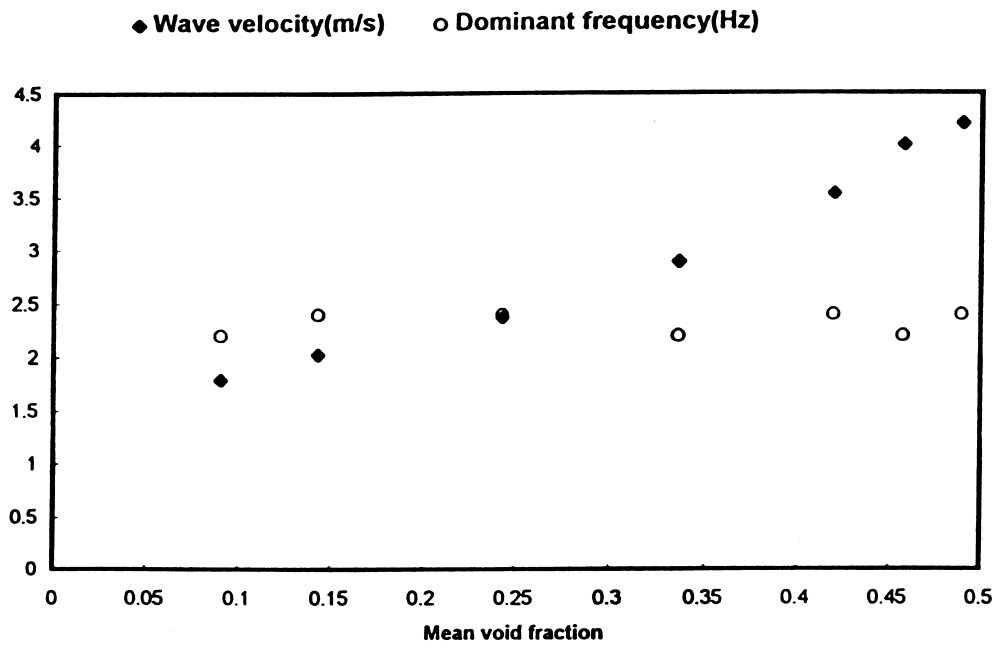

Figure 8. The variation of wave velocity and dominant frequency with void fraction at water velocity of 0.65 m/s. ◆ Wave velocity (m/s) ○ Dominant frequency (Hz).

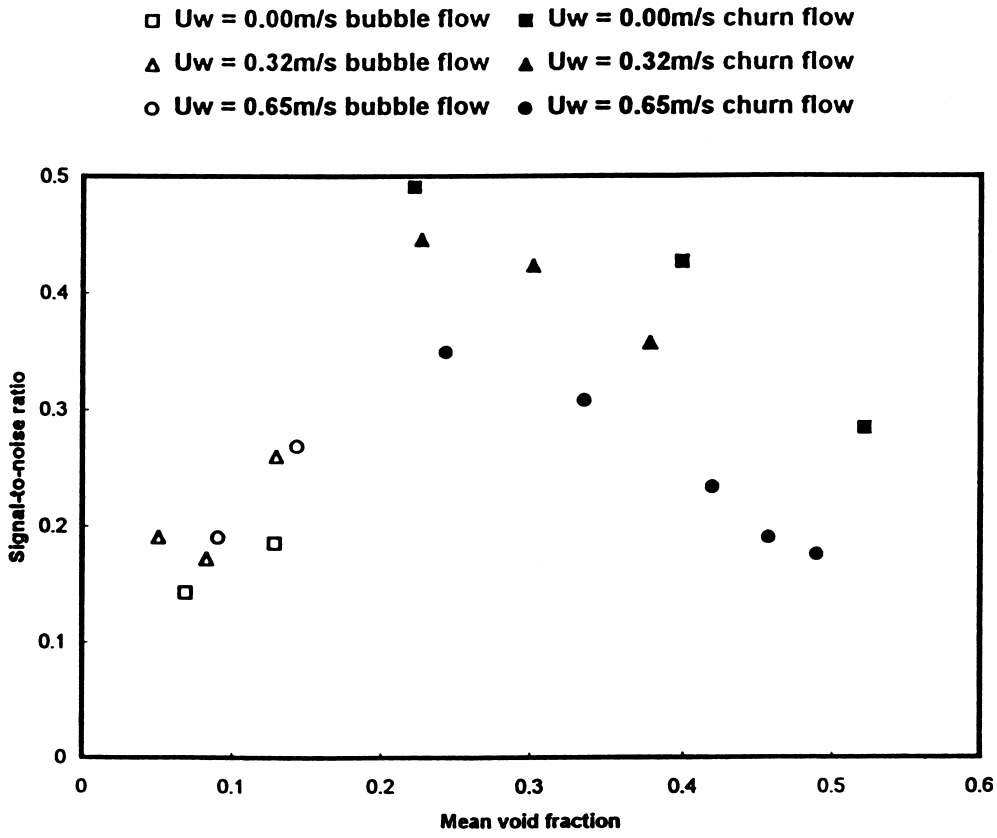

Figure 9. Signal-to-noise ratio of st. 2 at different water velocities. □ Uw = 0.00 m/s bubble flow; ■ Uw = 0.00 m/s churn flow; △ Uw = 0.32 m/s bubble flow; ▲ Uw = 0.32 m/s churn flow; ○ Uw = 0.65 m/s bubble flow; ● Uw = 0.65 m/s churn flow.

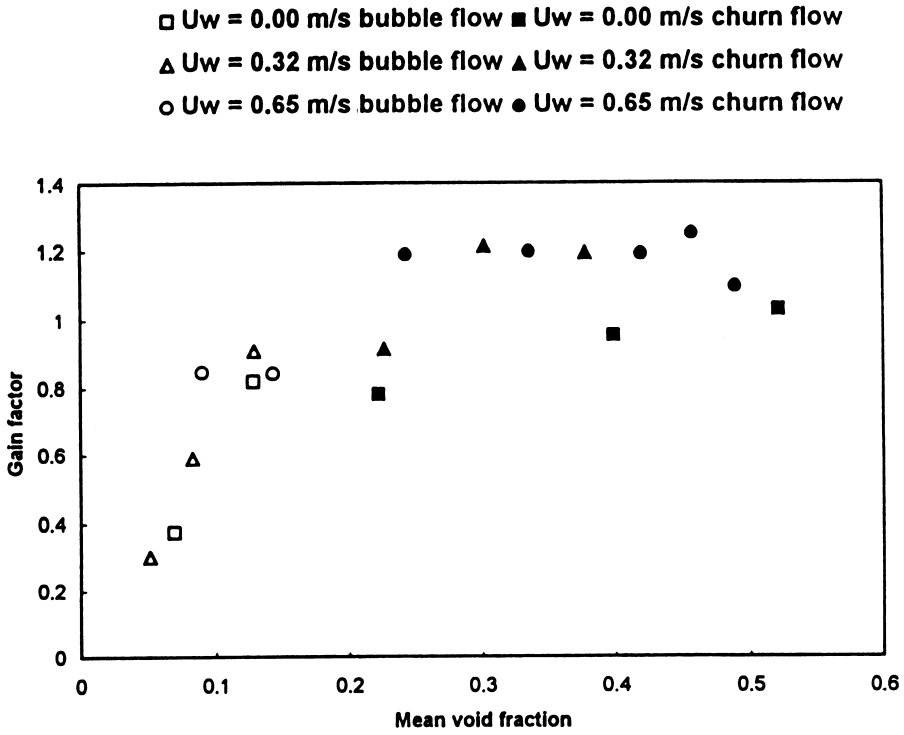

Figure 10. Gain factor at different water velocities. □ Uw = 0.00 m/s bubble flow; ■ Uw = 0.00 m/s churn flow; △ Uw = 0.32 m/s bubble flow; ▲ Uw = 0.32 m/s churn flow; ○ Uw = 0.65 m/s bubble flow; ● Uw = 0.65 m/s churn flow.

System gain factor and coherent function are function of wave frequency, and normally have a peak at around dominant frequency. The variations of the maximum gain factor and with void fraction are shown in figure 10. For bubble flow, the system gain factor is less than 1 and increases with void fraction, implying that the propagating void fraction waves are attenuated and the attenuation has a decreasing tendency as the void fraction increases. For churn flow, the system gain factor becomes greater than 1, implying that the void fraction waves have been amplified. The transition point corresponds to cap bubble flow at these three constant water velocities.

These results are similar to those recorded in the literature for large bubbles (Song *et al.* 1995a), or bubble clusters (Park *et al.* 1993), where the development of the flow has also been followed by increasing gas rate at constant liquid rate. The instabilities of void fraction wave appear to be associated with the transition from bubble-to-churn flow, as was also suggested by these workers. However, the flow pattern can be also changed from bubble flow to churn flow by decreasing the liquid flow rate at constant gas velocity, and this is discussed in the next section.

6.3. *Measurements of void fraction waves at constant gas velocity in 150 mm column*

Figure 11 is a typical set of PSD curves at constant gas velocity. Compared to the results at constant water velocity shown in figure 7, with increasing mean void fraction the PSD narrows much more sharply, and the peak moves towards low frequencies rather than remaining at a constant frequency. This variation of dominant frequency is brought out in figure 12 which also shows that the wave velocity decreases with increasing void fraction. Comparing figures 8 and 12 it is clear that it is not void fraction alone which determines wave velocity and frequency, but also the phase velocities. Thus the regions of high void fraction, which would become slugs in a narrower column, decrease in number and increase in length, as void fraction increases.

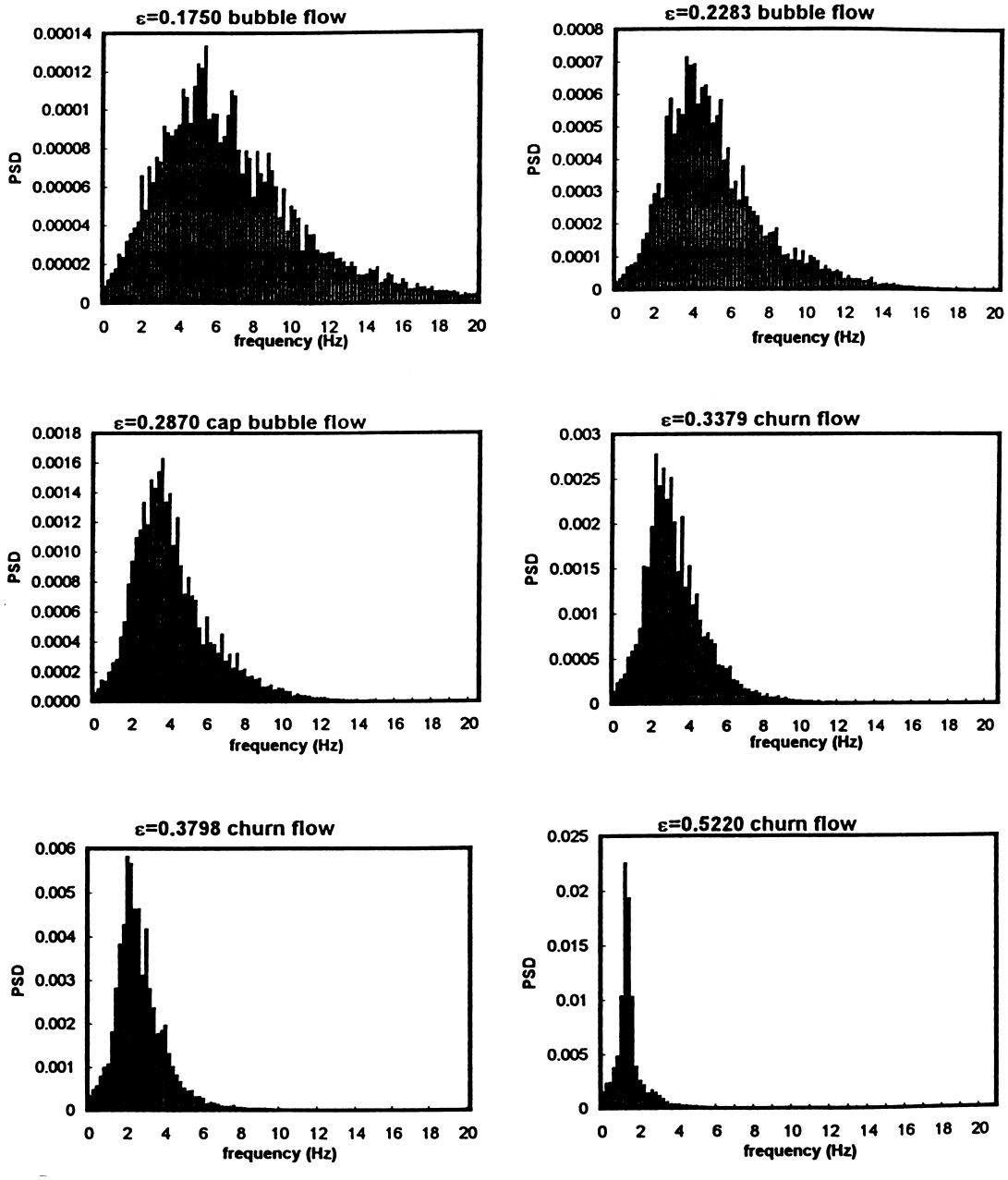

Figure 11. PSD plots at constant gas velocity of 0.7378 m/s.

Also unlike the experimental results at constant water velocity, the SNR does not go through a clear maximum but rather increases with void fraction (figure 13), and the system gain factor is always bigger than 1 with very little clear trend, in spite of the variation of flow pattern in the column (figure 14).

It would thus appear that the criteria suggested for detecting a transition from bubble-to-slug flow are not universally applicable in this 150 mm column.

The comparison of figures 8 and 12 showed that the dominant wave frequency remains unchanged with increasing void fraction for constant water velocity, and increases with increasing water velocity. Further investigation leads to figure 15, which shows that for all the flow conditions studied in the 150 mm diameter column, the dominant frequency depends linearly on the superficial water velocity only, independent of gas velocity in the range 0.03 to 1.66 m/s.

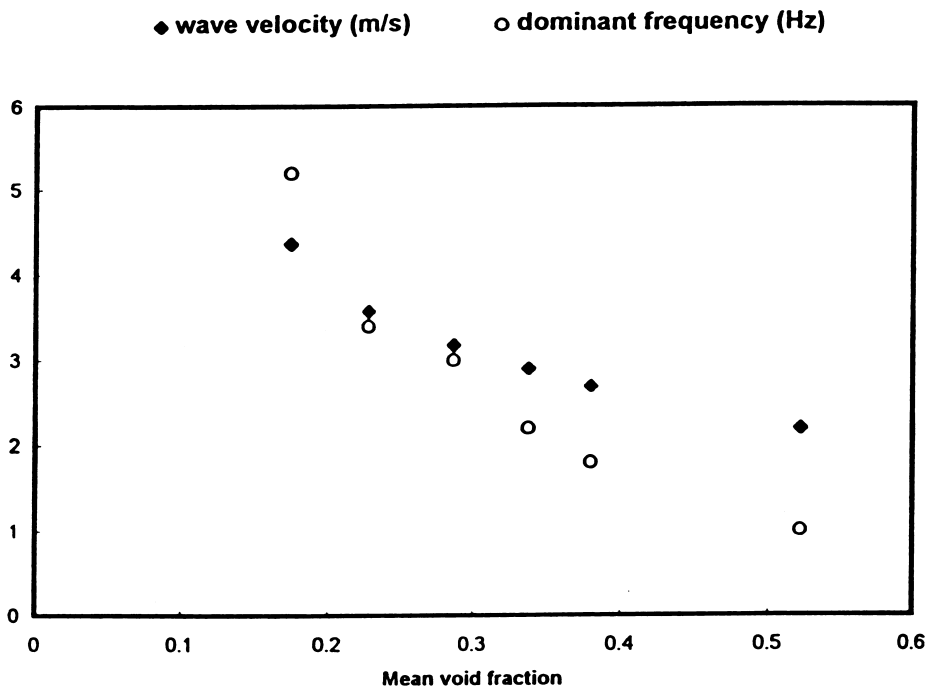

Figure 12. The variation of wave velocity and dominant frequency with void fraction at constant gas velocity of 0.7378 m/s. ◆ wave velocity (m/s); ○ dominant frequency (Hz).

The propagating wave velocity is compared with slug rising velocity calculated from available equations in the literature in figure 16. Like the slug rising velocity, propagating wave velocity is a linear function of mixture flow rate of the two-phase flow, but somewhat greater than the slug rising velocity calculated from these equations.

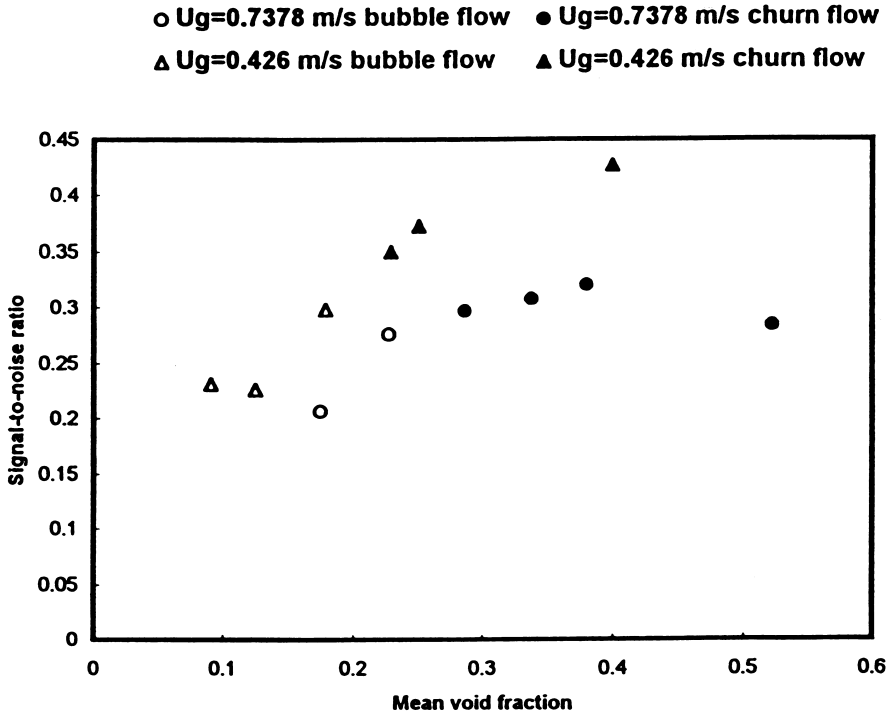

Figure 13. Signal-to-noise ratio at constant gas velocities. ○ Ug = 0.7378 m/s bubble flow; ● Ug = 0.7378 m/s churn flow; △ Ug = 0.426 m/s bubble flow; ▲ Ug = 0.426 m/s churn flow.

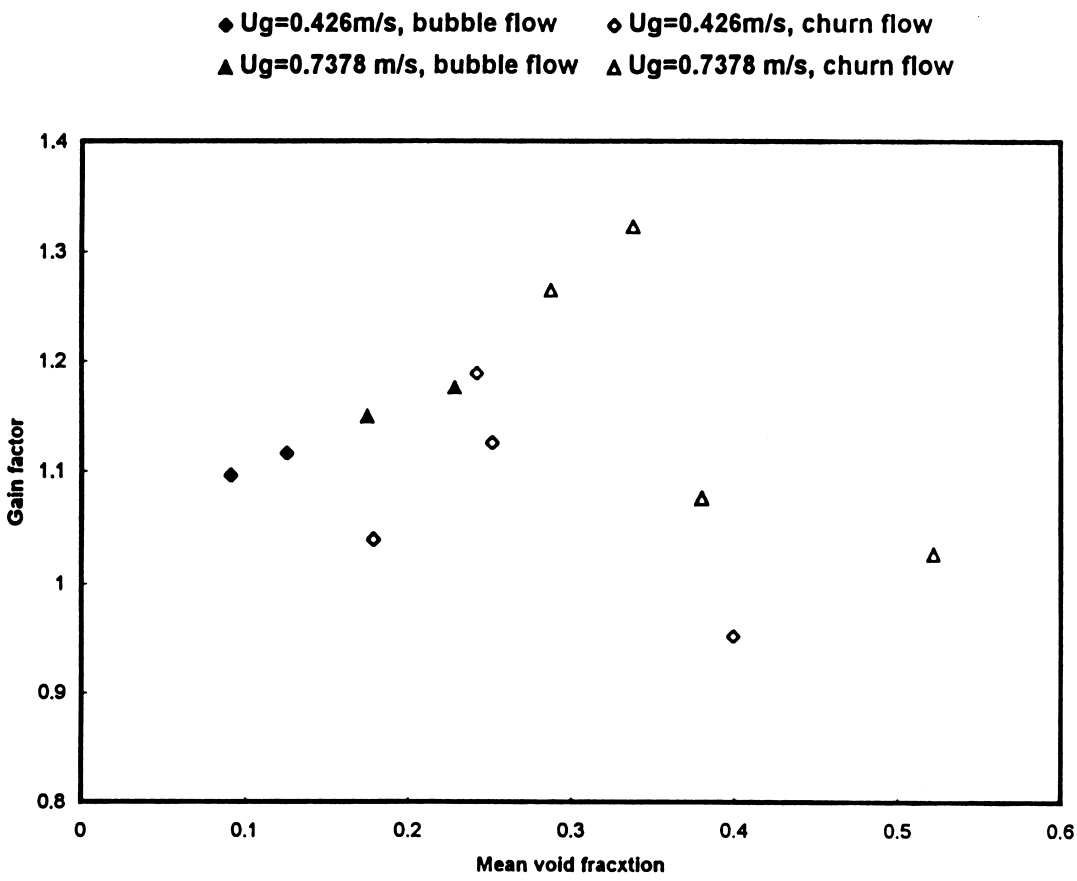

Figure 14. Gain factor at constant gas velocities. ◆ Ug = 0.426 m/s, bubble flow; ◇ Ug = 0.426 m/s, churn flow; ▲ Ug = 0.7378 m/s, bubble flow; △ Ug = 0.7378 m/s, churn flow.

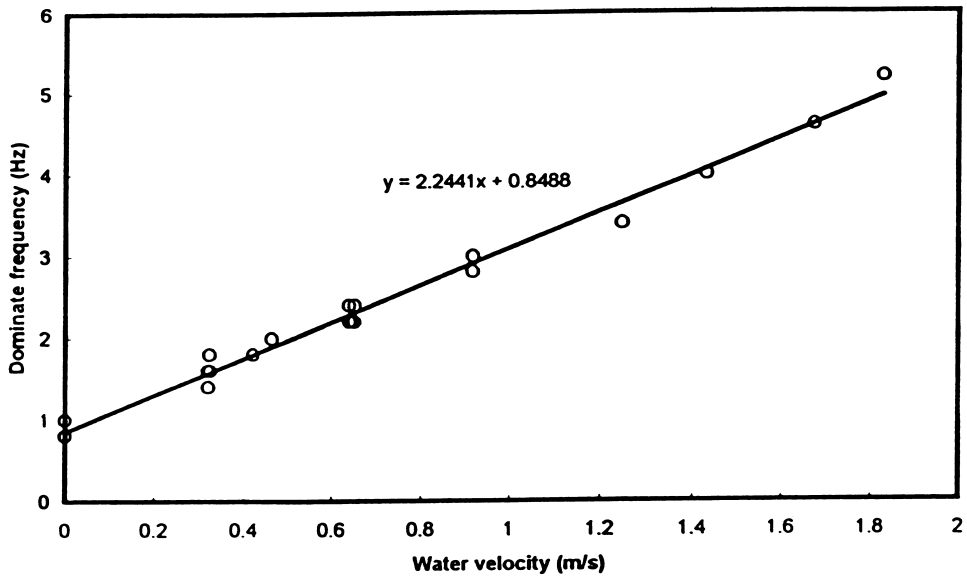

Figure 15. Dominant frequency against water velocity at different gas velocity (0.03–1.66 m/s).

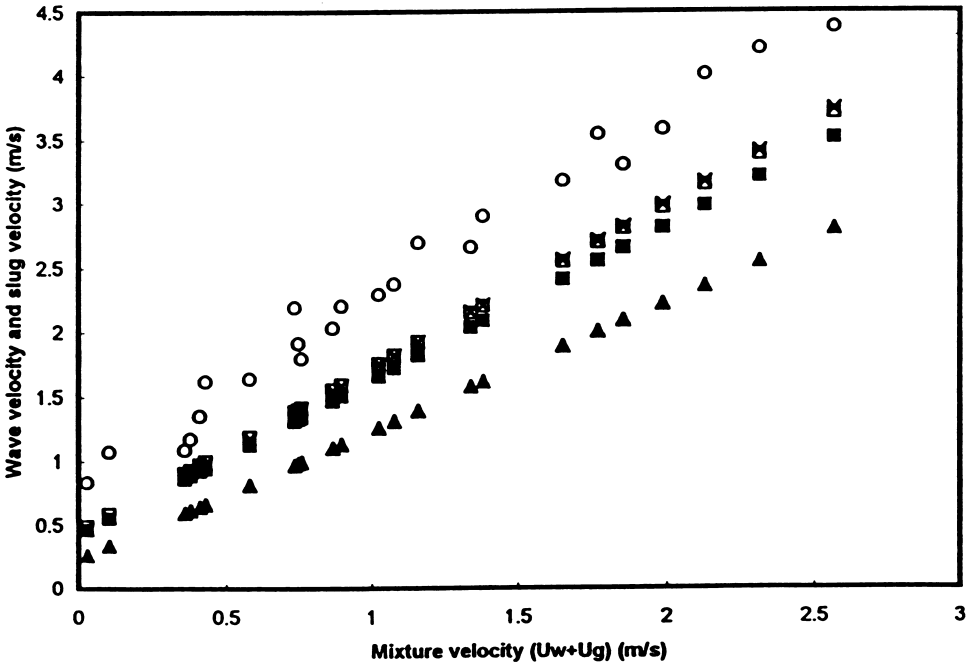

Figure 16. Comparing wave velocity with slug velocity calculated from different equations. ○, Experimental wave velocity; ■, Nicklin and Davidson (1962); X, Fernandes *et al.* (1983); □, Mao and Duckler (1985); ▲, Lisseter and Fowler (1992).

6.4. *Experiments of void fraction waves at constant water velocity of 0.65 m/s in 28.9 mm diameter column for relatively small bubble size*

At a constant water velocity of 0.65 m/s, with increasing gas velocity from 0.14 to 0.96 m/s, two typical flow regimes are observed. At void fraction of 0.07295 and 0.1058 (Run s01 and Run s02), discrete bubble flow is observed throughout the whole column, and the PDF plot of the wave signal shows a single narrow peak. As the void fraction increased to 0.17065 (Run s03), large bubble structures are observed from measuring station 3 upwards; these large bubble structures expand with height and develop into Taylor bubbles at the top of the column. As the gas flow rate increases further, the length of the slugs is increased. Accompanying the appearance of the large bubble structure, the PDF of the wave signal shows a single peak with a tail, and the tail becomes more and more pronounced and eventually develops into a second peak, as the mean void fraction increases. This is the classical behaviour reported in the literature. During these experiments, no obvious bubble cluster flow is observed.

The development of system gain factor and coherent function along the column for the given flow conditions are shown in figure 17. For discrete bubble flow, the system gain factor is less than 1, generally increasing with column height in a given run and with increasing mean void fraction from run to run. The coherent function is relatively low. For slug flow, the system gain factor is greater than 1, and the largest values occur in Run s03 where a large bubble structure (the origin of slug flow) is first spotted. The signals from two successive measuring stations become fully coherent in this case. At higher void fractions, the gain factor decreases somewhat, while remaining above 1, which agrees with observations in the literature (e.g. Park *et al.* 1993; Song *et al.* 1995a).

The variation of SNR with mean void fraction is illustrated in figure 18. There is a very rapid increase up the column in the two runs where the slug flow is developing (s03 & s04), which again corresponds to the observations of Song *et al.* (1995a).

More experiments on void fraction waves at different flow conditions are to be carried out in the 28.9 mm column. In particular, the effect of approaching the transition at constant gas rate will be studied, to compare with the results in the 150 mm diameter column. The effects of initial bubble size on the transition from bubble to slug will also be looked at.

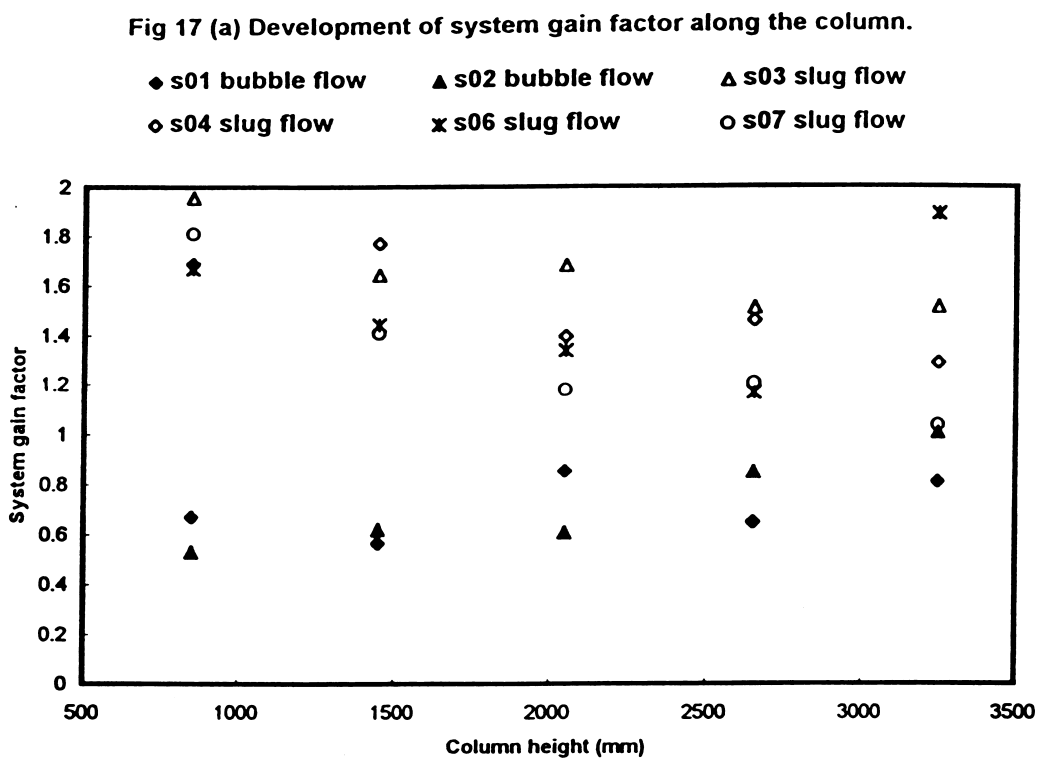

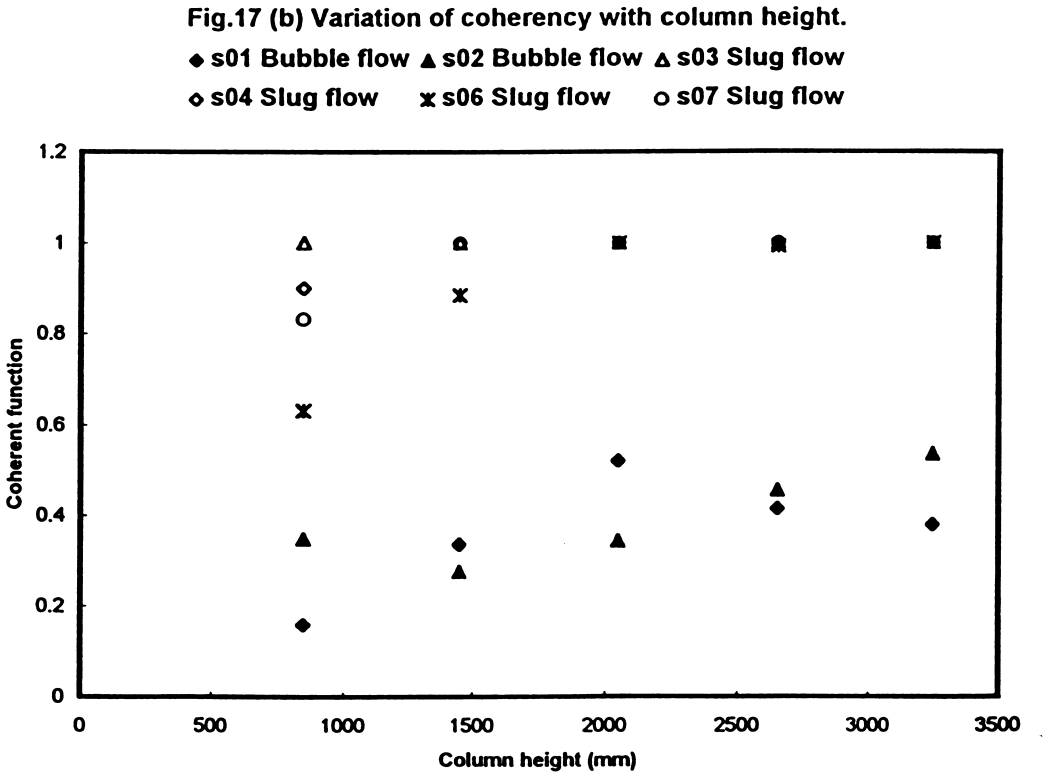

Figure 17. (a) Development of system gain factor along the column. ◆ s01 bubble flow; ▲ S02 bubble flow; △ s03 slug flow; ◇ s04 slug flow; ✱ s06 slug flow; ○ s07 slug flow. (b) Variation of coherency with column height. ◆ s01 Bubble flow; ▲ s02 Bubble flow; △ s03 Slug flow; ◇ s04 Slug flow; ✱ s06 Slug flow; ○ s07 Slug flow.

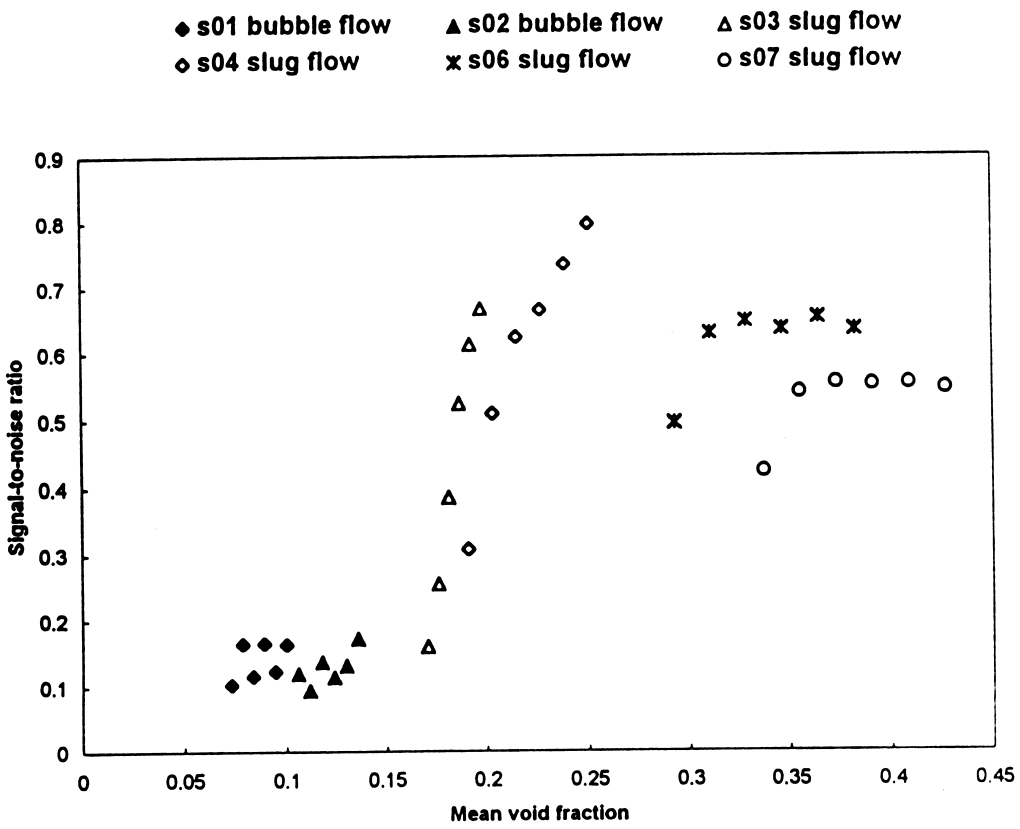

Figure 18. Variation of SNR with mean void fraction. ◆ s01 bubble flow; ▲ s02 bubble flow; △ s03 slug flow; ◇ s04 slug flow; ✱ s06 slug flow; ○ s07 slug flow.

7. CONCLUSIONS

- Traditional slug flow does not exist in our 150 mm diameter column. Instead, there is a very gradual transition to a type of churn flow as gas rate is increased.
- Bubble size, both mean and median chord lengths, decreases with height and the bubble frequency increases. This suggests bubble break-up rather than coalescence, although there is some evidence of an increase in the maximum size of cap bubbles found at high gas rates.
- When increasing gas rate at constant liquid rate in the 150 mm column, the gain factor gradually increases through 1.0, and the SNR passes through a maximum at the visually observed onset of large flow structures. There is no such obvious trend when the liquid rate is reduced at constant gas rate, and although the same transition is observed visually, the system gain factor remains above 1.0; gain factor alone is clearly not a suitable criterion for judging the transition.
- In the 28.9 mm column, increasing the gas rate at constant liquid rate leads to a sudden transition to slug flow, with a jump in the gain factor to $\rangle 1.0$, and also in the SNR. The suddenness of the transition would suggest an instability mechanism, rather than a gradual coalescence.
- The cause of the gradual transition in the 150 mm column remains unclear.

Acknowledgements—This work has been carried out under a Research Contract No. GR/J47392 from the EPSRC, whose support is gratefully acknowledged.

REFERENCES

Bendat, J. S. and Pierson, A. G. (1971) Random data: Analysis and Measurement Procedures, Wiley-interscience.

Bouré, J. A. (1988) Properties of Kinematic Waves in Two-Phase Pipe Flow Consequences on the Modelling Strategy, European two-phase flow group meeting, Brussels, 30 May–1st June.

Fernandes, R. C., Semiat, R. and Duckler, A. E. (1983) Hydrodynamic Model for Gas–Liquid Slug Flow in Vertical Tubes. *AIChE Journal* **29,** 981–989.

Hewitt, G. F. (1990) Non-equilibrium Two-phase Flow. In *Proc. 9th int. heat transfer conf., Jerusalem lecture, Jerusalem, Israel.* Vol. 1, pp. 383–394.

Hewitt, G. F. and Jayanti, S. (1993) To Churn or not to Churn. *Int. J. Multiphase Flow* **19,** 527–529.

Hills, J. H. (1976) The Operation of a Bubble Column at High Throughputs. I. Gas Holdup Measurements. *Chem. Eng. J.* **12,** 89–99.

Kapteyn, C. (1989) Measurements on Concentration Waves in Bubbly Liquids, Ph.D., Thesis, University of Twente.

Kytömaa, H. K. (1987) Stability of the structure in Multicomponent Flow, Ph.D. Thesis, California Institute of Technology.

Kytömaa, H. K. and Brennen, C. E. (1991) Small Amplitude Kinematic Wave Propagation in two-component Media. *Int. J. Multiphase Flow* **17,** 13–26.

Lisseter, P. E. and Fowler, A. C. (1992) Bubbly Flow-II; Modelling Void Fraction Waves. *Int. J. Multiphase Flow* **18,** 99–113.

Liu, T. J. (1993) Bubble Size and Entrance Length Effects on Void Development in a Vertical Channel. *Int. J. Multiphase Flow* **19,** 99–113.

Mao, Z. and Dickler, A. E. (1985) Rise Velocity of a Taylor Bubble in a Train of such Bubbles in a Flowing Liquid. *Chem. Engng, Sci.* **40,** 2158–2160.

Matuszkiewicz, A., Flamand, J. C. and Bouré, J. A. (1987) The Bubble-slug Flow Pattern Transition and Instabilities of Void Fraction Waves. *Int. J. Multiphase Flow* **13,** 199–217.

Micaelli, J. C. (1982) One Dimensional Modelling of Bubble Flow by a Stochastic Analysis of the Gaseous Phase Behaviour: Void Fraction Waves Model stability, *Proc. of the Ninth U.S. National Congress of Applied Mechanics*, Held at Cornell University, ITHACA, New York, 21–25 June, Pao, Y.H., ed. Comm. Chairman, ASME, 93–100.

Monji, H. (1993) Transition Mechanism from Bubble Flow to Slug Flow in a Riser. *Fluid Dynamics Research* **11,** 61–74.

Nicklin, D. J. and Davidson, J. F. (1962) The Onset of Instability in Two-phase Slug Flow, Proc. I. Mech. Engineers on Symposium on Two-phase Fluid Flow, 29–34.

Park, J. W. (1992) Void Wave Propagation in Two-Phase Flow, Ph.D. Thesis, Rensselaer Polytechnic Institute.

Park, J. W., Lahey, R. T. Jr. and Drew, D. A. (1993) The Measurement of Void Waves in Bubbly Two-phase Flows, Proc. 6th Int. MTG. on Nuclear Reactor Thermal-Hydraulics, Grenoble, 5–8 Oct., 655–662.

Radovcich, N. A. and Moissis, R. (1962) The Transition from Two-phase Bubble Flow to Slug Flow, MIT Report, Report No. 7-7673-22.

Saiz-Jabardo, J. M. and Bouré, J. A. (1989) Experiments on Void Fraction Waves. *Int. J. Multiphase Flow* **15,** 483–493.

Serizawa, A. (1984) Personal communication, also referred to in Serizawa *et al.* (1988).

Serizawa, A. and Kataoka, I. (1987) Phase Distribution in Two-phase Flow. In *Proc. Transient Phenomena in Multiphase Flow, ICHMT, Int. Seminar, Dubrovnik, Croatia*, pp. 179–224.

Serizawa, A., Kataoka, I., Zun, I. and Michiyoshi, I. (1988) Bubble Size Effect on Phase Distribution, Proc. of the Japan-US Seminar on Two-phase flow Dynamics, pp. 15–20.

Serizawa, A., Kataoka, I. and Gofuku, A. (1991) Effects of Initial Bubble Size on Bubbly Flow Structure, Proc. of the International Conference on Multiphase Flows '91, September 24–27, Tsukuba, Japan.

Song, C. H., No, H. C. and Chung M. K. (1995a) Investigation of Bubble Flow Developments and its Transition Based on the Instability of Void Fraction Waves. *Int. J. Multiphase Flow* **21**, 381–404.

Song, C. H., Chung, M. K. and No, H. C. (1995b) The Effect of Bubble Flow Structures on the Void Wave Propagation in a Large Diameter Pipe, Proc. of the 2nd International Conference on Multiphase Flow '95, 3–7 April, Kyoto, Japan.

Taitel, Y., Bornea, D. and Dukler, A. E. (1980) Modelling Flow Pattern Transition for Steady upward Gas-liquid Flow in Vertical Tubes. *AIChE Journal* **26,** 345–353.

Tournaire, A. (1987) Détection et Etude des Taux de vide en Ecoulements Diphasiques à Bulles jusqu'à la Transition Bulles-Bouchons. Ph.D. thèse, Université Scientifique et Médicale et Institut National Polytechnique de Grenoble, France.

Wallis, G. B. (1969) One-dimensional Two-phase Flow, McGraw Hill.